# Reconnaissance investigation of magnetite trace-element compositions from the New Afton Cu-Au deposit, British Columbia

J.A. Percival[1]*, E. Schetselaar[1], D.C. Petts[1], S.E. Jackson[1], and D. Wade[2]

*Percival, J.A., Schetselaar, E., Petts, D.C., Jackson, S.E., and Wade, D., 2020. Reconnaissance investigation of magnetite trace-element compositions from the New Afton Cu-Au deposit, British Columbia;* in *Targeted Geoscience Initiative 5: contributions to the understanding and exploration of porphyry deposits, (ed.) A. Plouffe and E. Schetselaar; Geological Survey of Canada, Bulletin 616, p. 91–108. https://doi.org/10.4095/327990*

**Abstract:** Abundant magnetite occurs sporadically in variable textural settings within the New Afton Cu-Au porphyry deposit. A study to test the utility of magnetic anomalies as an exploration vector was conducted by analyzing magnetite in drill core samples from a variety of rock types and alteration facies. Magnetite samples from various settings (i.e. disseminated, isolated, vein, breccia grains) were analyzed by a laser-ablation inductively coupled plasma-mass spectrometer for iron and trace elements. New Afton magnetite compositions were compared to previously defined compositional fingerprints of porphyry, iron oxide copper gold, skarn, polymetallic vein, and layered intrusion deposit types. On multi-element plots using bulk continental crust as the normalizing factor, most New Afton magnetite analyses plot within the high-temperature hydrothermal magnetite field, although most samples have elevated V and 6 of 19 samples have notably higher W than other deposit types. A hydrothermal origin is supported by a Ti versus Ni-Cr plot, which discriminates hydrothermal from magmatic magnetite; however, a Ti versus V plot suggests mainly magmatic compositions. Copper is generally depleted relative to bulk crust; gold and platinum values are near their detection limits. Veins, one of the main magnetite habits, define brittle fracture patterns, and trace-element characteristics support formation by pulses of oxidized, high-temperature hydrothermal fluid. The texture and composition of the samples suggest that magnetite crystallized from late magmatic fluids that drove porphyry mineralization.

**Résumé :** Dans le gisement porphyrique à Cu-Au de New Afton, on trouve de grandes quantités de magnétite distribuées sporadiquement dans des contextes texturaux variés. Afin de vérifier si les anomalies magnétiques pouvaient servir de vecteur d'exploration, nous avons analysé la magnétite présente dans des échantillons de carottes de forage recoupant divers types de roches et de faciès d'altération. Nous avons utilisé un spectromètre de masse avec plasma à couplage inductif jumelé à l'ablation par laser pour doser le contenu en fer et en éléments en traces de la magnétite présente dans divers contextes texturaux (c.-à-d. grains disséminés, isolés, dans des filons ou dans des brèches). La composition des grains de magnétite du gisement de New Afton a été comparée aux caractéristiques compositionnelles déterminées antérieurement pour d'autres types de gîtes minéraux : gîtes porphyriques, gîtes d'oxydes de fer–cuivre-or, skarns, gîtes filoniens à minéralisation polymétallique et gîtes associés à des intrusions stratifiées. Dans des diagrammes multiéléments où les valeurs mesurées sont normalisées à la composition globale de la croûte continentale, la majeure partie des résultats d'analyse de la magnétite du gisement de New Afton se situent dans le champ de la magnétite hydrothermale de haute température, bien que la plupart des échantillons contiennent des teneurs élevées en V et que 6 échantillons sur 19 ont des teneurs nettement plus élevées en W que celles relevées dans d'autres types de gîtes. Une origine hydrothermale est appuyée par le diagramme de Ti en fonction du rapport Ni/Cr qui permet de distinguer la magnétite d'origine hydrothermale de celle d'origine magmatique. Toutefois, le diagramme de Ti en fonction de V suggère des compositions surtout magmatiques. Le cuivre est généralement appauvri par rapport à la composition globale de la croûte, et les concentrations d'or et de platine sont près de leur seuil de détection. Les filons, l'un des principaux modes d'occurrence de la magnétite, définissent des configurations de fracturation fragile, tandis que les caractéristiques des éléments en traces appuient une formation de ceux-ci par des impulsions de fluides hydrothermaux oxydés de haute température. La texture et la composition des échantillons suggèrent que la magnétite a cristallisé à partir de fluides magmatiques de phase tardive qui ont produit la minéralisation porphyrique.

[1]Geological Survey of Canada, 601 Booth Street, Ottawa, Ontario K1A 0E8
[2]New Gold Inc., 4050 West Trans-Canada Highway, Kamloops, British Columbia V1S 2A3
*Corresponding author: J.A. Percival (email: john.percival@canada.ca)

## INTRODUCTION

Porphyry deposits are generated by granitoid magmatism, but a specific series of processes, from magma generation through fractionation and emplacement, needs to align to concentrate metals into ore deposits. It is well established that oxidizing conditions are required during melting to mobilize metals from mantle reservoirs (e.g. Mungall, 2002; Sillitoe, 2002, 2010; Richards, 2009, 2011a, b; Cooke et al., 2014), and that subsequent fractionation and metal behaviour are determined by magma oxidation state and volatile content.

Magnetite is one of the most obvious indicators of a highly oxidized magma; however, magnetite is uncommon in many porphyry districts and as a result, indirect indicators of oxidation state, such as rare-earth–element distribution in zircon (Ballard et al., 2002; Zhong et al., 2019), have been used to evaluate the prospectivity of plutonic complexes. In this paper, we explore the relationship of widespread magnetite in the New Afton porphyry Cu-Au deposit to magmatic and alteration processes, with a view to defining its utility as an exploration vector within the host Iron Mask batholith.

## GEOLOGICAL SETTING

Situated in the Quesnel terrane of south-central British Columbia, the New Afton deposit is one of ten known porphyry deposits associated with the Iron Mask batholith (Sinclair, 2007; Logan and Mihalynuk, 2014). The Late Triassic (ca. 204 Ma; Mortensen et al., 1995), silica-saturated, alkalic, diorite-monzonite complex intrudes volcanic and associated sedimentary rocks of the Nicola Group. Copper-gold mineralization in the New Afton deposit is hosted by fragmental volcanic rocks of the Nicola Group and locally by the Cherry Creek monzonite phase of the Iron Mask batholith (J. Lipske and D. Wade, unpub. rept., 2014). The deposit is bounded partly by a thick picritic unit of the Nicola Group, and partly by north-northwest– and northeast-striking faults. It is also cut by faults of variable orientation, some of which may have channelled mineralizing fluids.

Several alteration facies are recognized with broadly concentric distribution in the New Afton deposit. Central zones of potassic (mainly biotite-dominant, with some K-feldspar–dominant patches) and calcic (magnetite-actinolite-apatite; epidote) alteration are surrounded by outer propylitic alteration. Late, structurally controlled phyllic alteration overprints the potassic and outer propylitic alteration along high-angle fault zones (Bergen et al., 2015; Tolman and Lipske, 2016). In general, protoliths can be identified in spite of the pervasive alteration.

## SAMPLING STRATEGY

To explore the role of magnetite in the New Afton porphyry system, magnetite-bearing samples were collected from drill core through different facies of the deposit (Fig. 1, 2). Rock types included fragmental volcanic rocks, Cherry Creek monzonite, and Pothook diorite with variable alteration facies (Table 1). Two main magnetite textural settings were recognized in the field and confirmed petrographically (Fig. 3): finely disseminated and vein (including brecciated veins).

## METHODS

Thick polished sections were cut from drill core, photographed, and imaged by a scanning electron microscope in back-scattered electron (BSE) mode. Images were used to select spots for analysis for iron and 36 trace elements by laser-ablation inductively coupled plasma-mass spectrometry (LA-ICP-MS). Beam sizes between 40 and 65 μm were used to ablate nominally inclusion-free material from representative grains of each textural type. A total of 106 analyses were obtained from 19 samples.

Analyses were calibrated using primary standard USGS GSD-1G (Jochum et al., 2007) analyzed with a 50 μm beam. A secondary standard, USGS BCR-2G (Jochum et al., 2007), was analyzed repeatedly during the analytical sessions for quality control purposes. The LA-ICP-MS data were processed using GLITTER (Griffin et al., 2008), using 'GeoReM preferred values' (Jochum, et al., 2005) for elemental contents in GSD-1G and the stoichiometric Fe content of magnetite (approximately 723 600 ppm) for internal standardization. The detection limit varies by element and several elements are consistently near or below detection (5–10 ppb): Pd, Ag, Re, Pt, and Au. Precision and accuracy, assessed via repeated analysis of BCR-2G, are estimated at better than 5% for most elements.

Data were plotted on plots designed to distinguish magnetite in various mineralized environments. Dare et al. (2014) presented comparative data from a number of mineral deposit types, whereas other authors have developed discriminative methods relevant to porphyry deposits (Nadoll et al., 2014, 2015).

## RESULTS AND DISCUSSION

Magnetite from New Afton contains low contents of Cu and Au (Appendix A), contributing little to the ore metal budget. The content of Mg, Al, Si, Ca, Ti, V, Cr, and W ranged from 0.01 ppm to more than 1000 ppm, with median values of 870, 2660, 1695, 236, 4120, 3250, 21, and 0.6 ppm, respectively. Maximum P, Mn, Co, Ni, and Zn values fall in the range of 100 to 1000 ppm (median values of 3, 434, 48, 89, and 195 ppm, respectively). The highest values

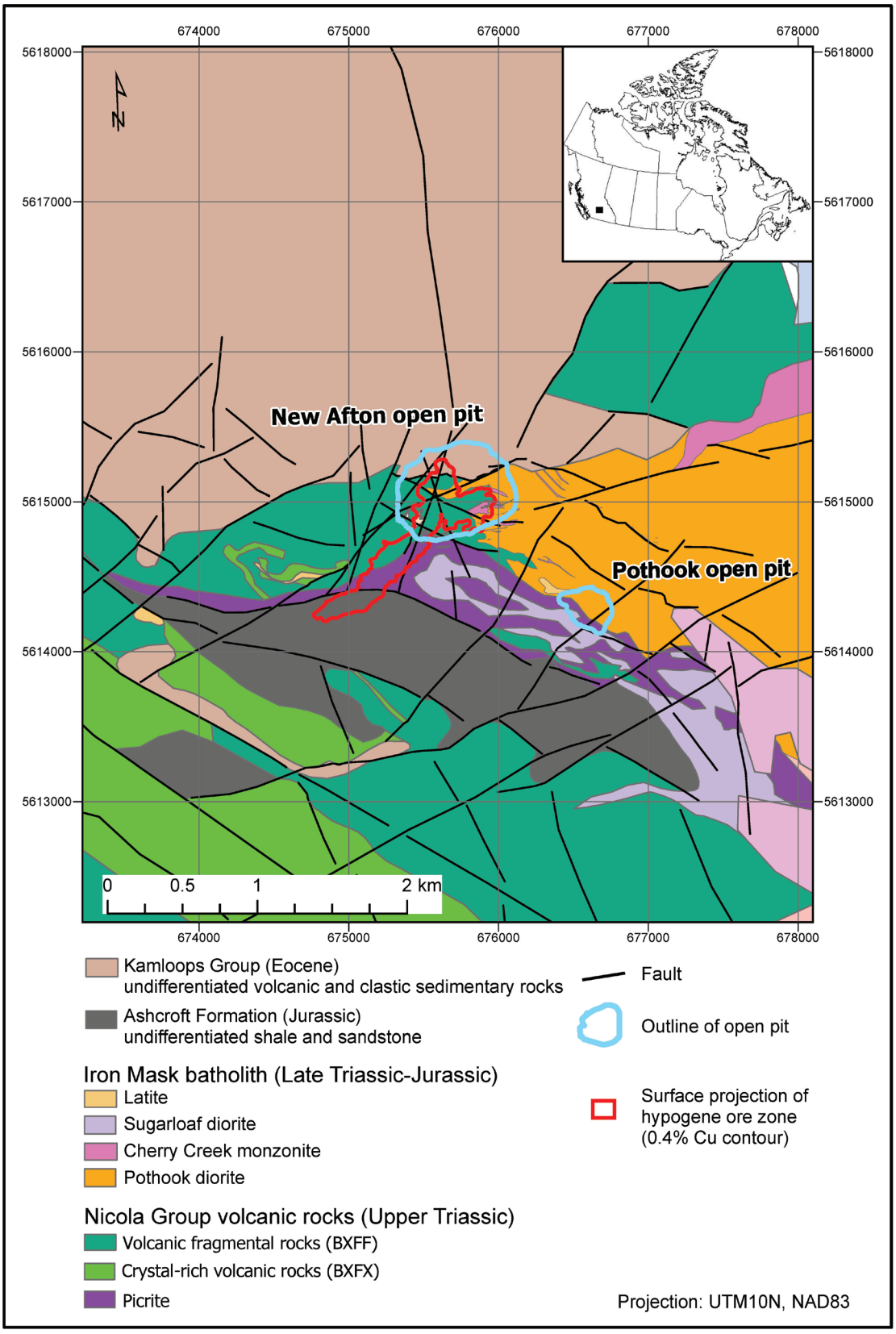


**Figure 1.** Geological setting of the New Afton deposit (Bergen et al., 2015; Logan et al., 2006).

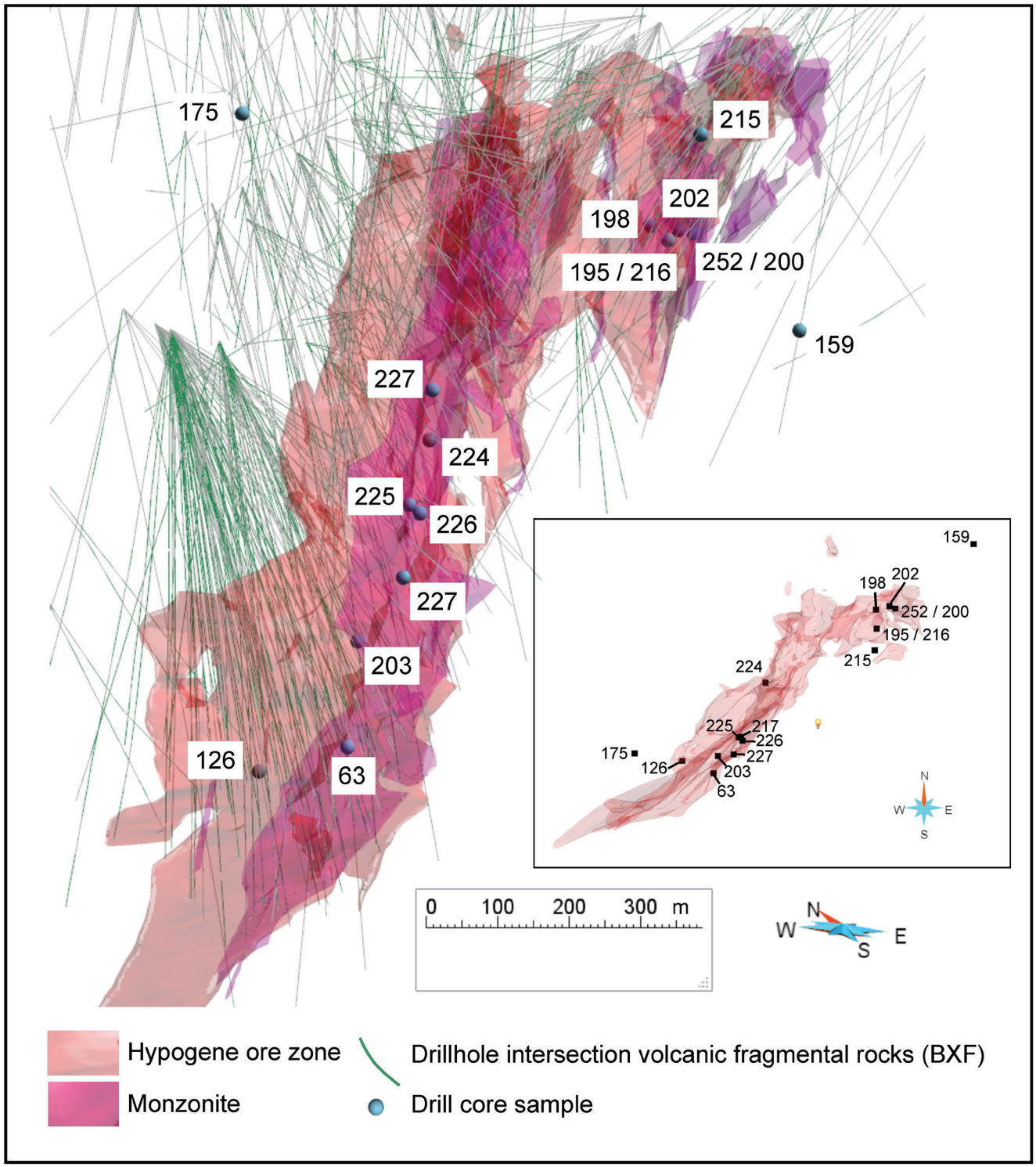


**Figure 2.** Three-dimensional projection of the spatial distribution of samples from the New Afton ore zone and surrounding area analyzed in this study. Inset map shows plan view of drill core sample locations and hypogene ore zone.

**Table 1.** Locations and petrographic descriptions of magnetite-bearing samples from the New Afton copper-gold porphyry deposit.

| Sample number | Hole identifier | Depth (m) | Rock type | Alteration type | Magnetite habits |
|---|---|---|---|---|---|
| 63 | EA14-133 | 671.50 | Monzonite | Potassic (K-feldspar) | Thick, vein-brecciated, fibrous |
| 126 | EA17-187 | 484.84 | Volcanic fragmental | Potassic (K-feldspar) | Magnetite-apatite veins cut by younger quartz veins |
| 159 | AF06-94 | 744.95 | Volcanic fragmental mafic volcanic | Potassic (K-feldspar) | Thick magnetite-apatite vein and disseminated in host rock |
| 175 | AF03-83 | 272.97 | Diorite | Phyllic | Thick magnetite-apatite vein and disseminated in host rock |
| 195 | EA13-058 | 299.36 | Monzonite (trachytic) | Potassic (K-feldspar) | Disseminated fine magnetite |
| 198 | ES13-059 | 339.82 | Volcanic fragmental crystal-lithic volcanic | Biotite (potassic) and propylitic | Thin veins and disseminated magnetite |
| 200 | ES13-060 | 332.04 | Volcanic fragmental crystal-rich | Biotite (potassic) and propylitic | Thin veins and peripheral disseminated |
| 202 | ES13-069 | 329.98 | Volcanic fragmental crystal-rich | Biotite (potassic) and propylitic | Brecciated magnetite veins; hypogene mineralization |
| 203 | EA14-125 | 454.96 | Highly altered monzonite? | Potassic (K-feldspar) | Brecciated thin magnetite veins |
| 215 | AF08-146 | 356.90 | Monzonite, plagioclase porphyritic | Potassic (K-feldspar) | Disseminated |
| 216 | AF08-146 | 357.70 | Monzonite, plagioclase porphyritic | none | Disseminated |
| 217 | UA05-44 | 384.68 | Monzonite, coarse grained | Potassic (K-feldspar), propylitic | Disseminated |
| 224 | EA13-42 | 177.00 | Monzonite, monzonite dykes | none | Magnetite-apatite vein |
| 225 | EA12-008 | 445.40 | Monzonite | Phyllic | Veins, breccia. Late hematite |
| 226 | EA12-008 | 465.30 | Monzonite, diorite xenolith | Potassic (K-feldspar) | Disseminated, sigmoidal vein |
| 227 | EA14-138 | 412.06 | Monzonite | Potassic (K-feldpar) | Brecciated vein, peripheral disseminated |
| 252 | WC17-002 | 304.61 | Fresh diorite | none | Magnetite-epidote vein; disseminated |
| 253 | WC17-002 | 225.55 | Fresh diorite, medium grained | none | Disseminated |
| 254 | WC17-002 | 128.70 | Monzonite dyke | none | Thin, discontinuous magnetite veins |

for Cu, Ga, Y, Zr, Mo, Sn, Sb, Ba, and Pb are between 10 and 100 ppm (median values of 0.9, 24, 0.8, 1.7, 0.3, 1.4, 0.3, 3, and 1.8 ppm, respectively). Maximum Ge, Se, Nb, and Hf contents are between 1 and 10 ppm (median 1.2, 0.3, 0.3, and 0.1 ppm, respectively). The median Ta content is 20 ppb, and Pd, Ag, Te, Re, Pt, and Au occur near the limit of detection during the analytical session. Local anomalous Mg, Si, Al, Ca, and P likely reflect inclusions of amphibole, quartz, feldspar, and apatite in the analyzed magnetite; these analyses, identified in Appendix A, are particularly common in the generally fine, disseminated magnetite grains.

To evaluate compositional variability within and among samples, bivariate element plots were produced. The Ti versus Ni-Cr plot in Dare et al. (Fig. 4a; 2014) is designed to discriminate magmatic from hydrothermal compositions. In this plot, both the disseminated and vein magnetite New Afton samples occur within the hydrothermal field; however, on a Ti versus V plot (Fig. 4b), New Afton magnetite samples with both habits fall within the magmatic field for porphyry deposits as defined by Nadoll et al. (2015), although a substantive subset of disseminated magnetite analyses occur within the overlapping portion of the hydrothermal magnetite field.

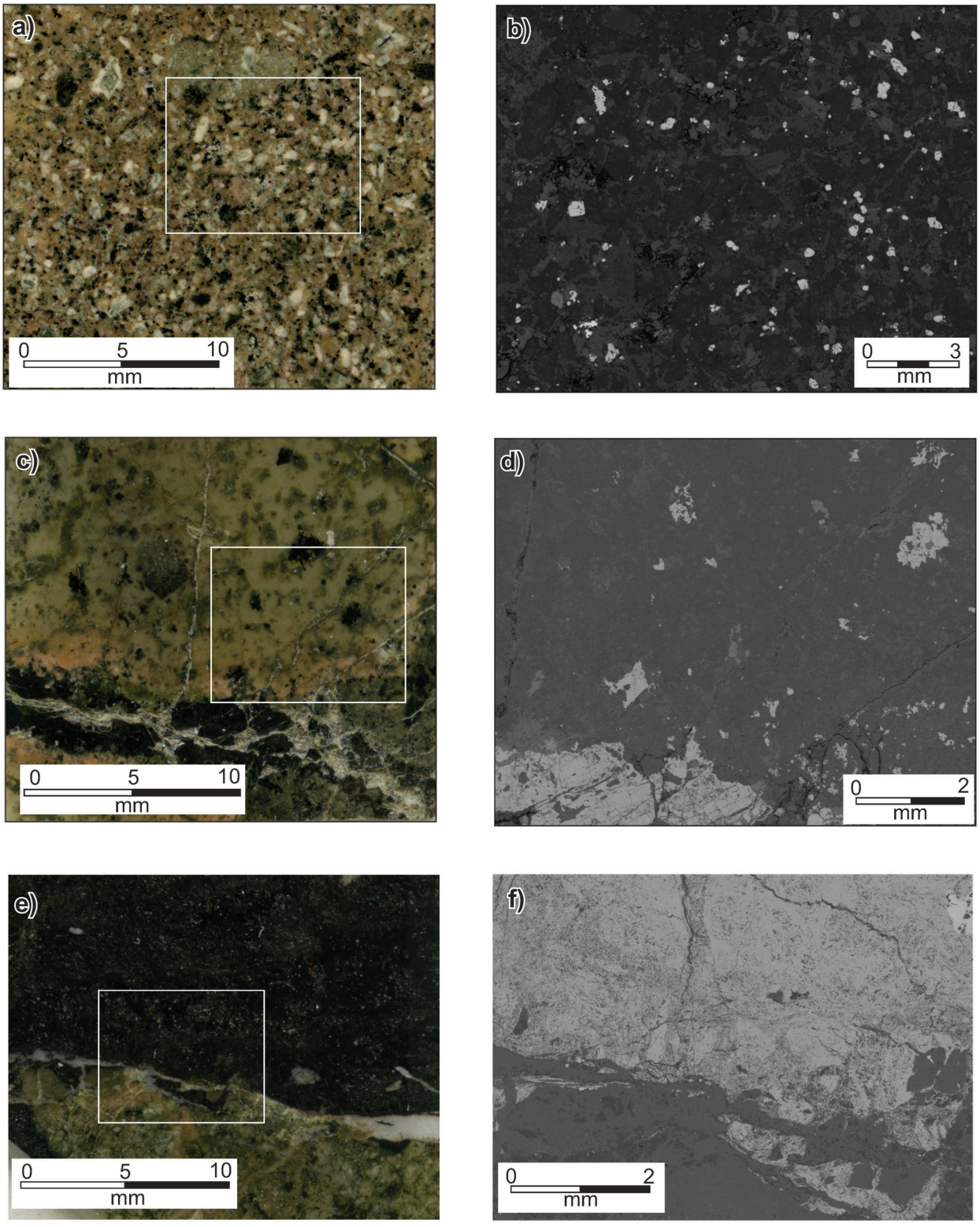


**Figure 3.** Polished surface and corresponding back-scattered electron (BSE) images of representative magnetite textures in the New Afton ore zone: **a)** polished surface of plagioclase porphyritic monzonite sample 216; **b)** BSE image of the white-outlined area in a) showing disseminated magnetite (light grey) in a well-preserved igneous matrix; **c)** polished surface of altered (biotite potassic, propylitic) fragmental volcanic sample 198 hosting vein and disseminated magnetite; **d)** BSE image of the white-outlined area in c) showing vein magnetite (lower left) and disseminated grains; **e)** polished surface of phyllic-altered diorite sample 175 with a thick magnetite-apatite vein; **f)** BSE image of the white-outlined area in e) showing a coarse magnetite (light grey) vein.

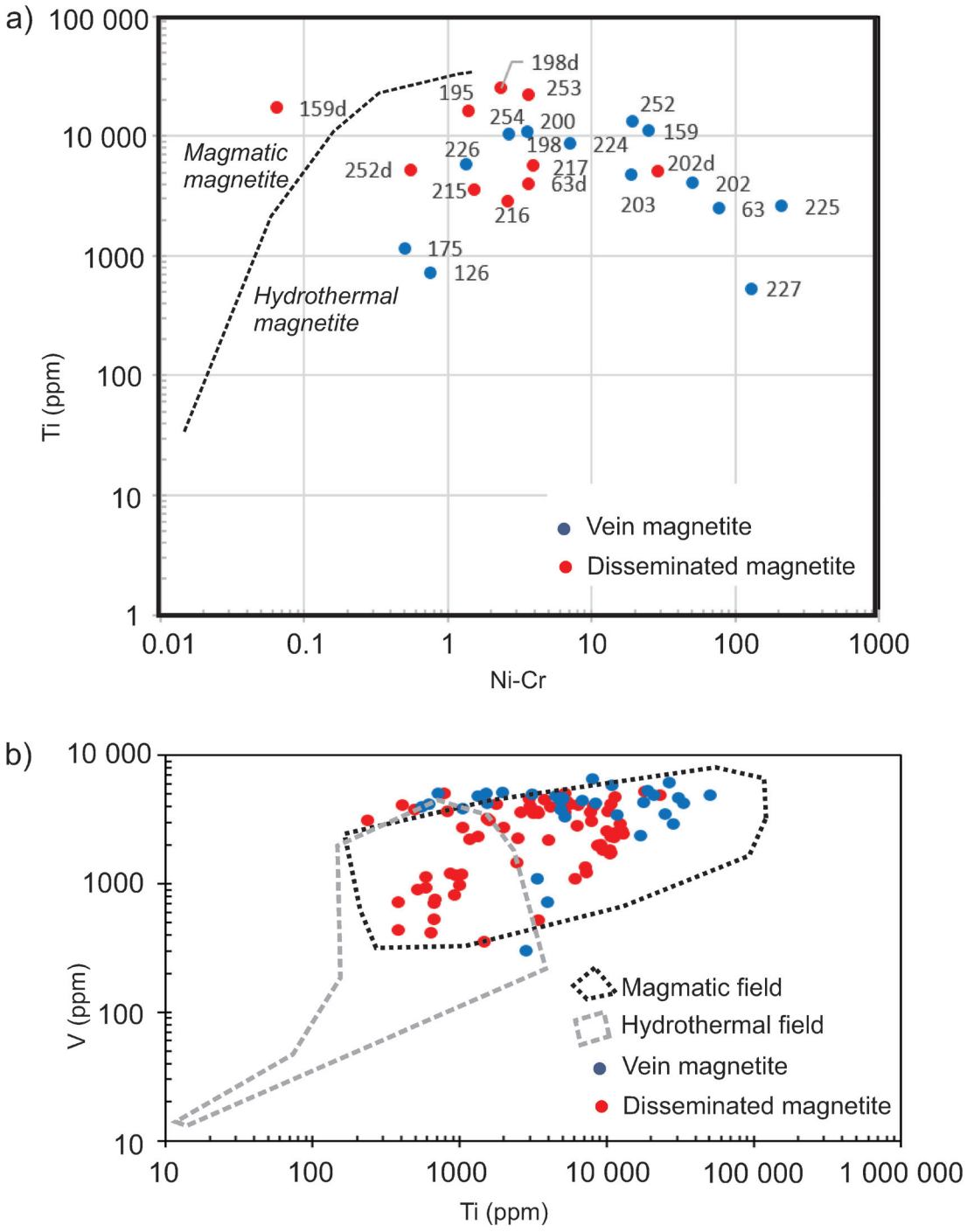


**Figure 4.** Discrimination plots showing trace-element content of New Afton disseminated and vein magnetite: **a)** Ti content versus Ni-Cr ratio of representative disseminated and vein samples. Fields defining magmatic and hydrothermal magnetite are after Dare et al. (2014); **b)** Ti content versus V content for all magnetite analyses. Fields defining magmatic and hydrothermal magnetite are based on a global compilation of porphyry deposits (*after* Nadoll et al., 2015).

Multi-element plots (Fig. 5, Appendix B) were constructed using the method of Dare et al. (2014), by normalizing analyses to average continental crustal values (Rudnick and Gao, 2003). Both disseminated (Fig. 5a) and vein (Fig. 5b) magnetite compositions from New Afton generally overlap the hydrothermal field, although V content systematically exceeds or falls within the upper reaches of the field for both textural types, matching the high V content of andesites reported by Dare et al. (2014). Niobium and copper values fall near the bottom or below the hydrothermal field limit and, in a few vein samples, magnetite is enriched in W by two orders of magnitude beyond the hydrothermal envelope.

Based on a global compilation, Huang et al. (2019) recognized significant variation in magnetite composition among different types of porphyry deposits based on multivariate statistical analysis of electron microprobe and LA-ICP-MS trace-element data. A combination of variables including origin (magmatic versus hydrothermal), magma composition, fluid composition, oxygen, and sulfur fugacity controls magnetite trace-element signatures. Huang et al.

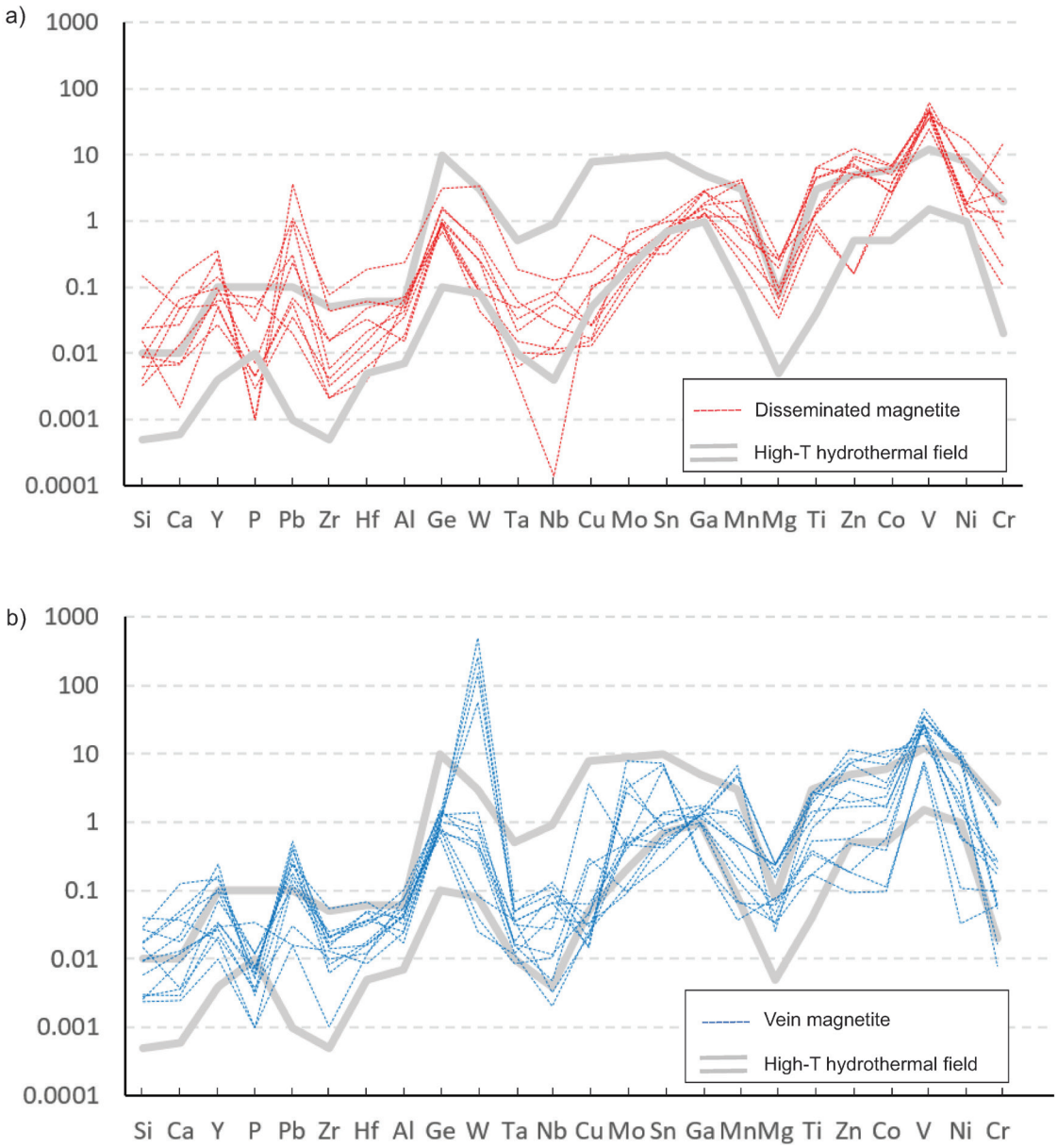


**Figure 5.** Multi-element (spider) plots showing New Afton magnetite analyses and the reference field for high-temperature hydrothermal magnetite compositions, *after* Dare et al. (2014): **a)** average analyses for disseminated magnetite; **b)** average analyses for vein magnetite.

(2019) found that, in general, magnetite of magmatic origin contains relatively high levels of P, Ti, V, Mn, Zr, Nb, Hf, and Ta, accompanied by generally low Mg, Si, Co, Ni, Ge, Sb, W, and Pb, owing to magnetite-magma partition coefficients. Both disseminated and vein magnetite from New Afton match some of these characteristics — high Ti and V with low Mg, Si, Co, and Ni — but they differ significantly in others — low Zr, Hf, Nb, and Ta, and high W and Pb. Tungsten, which appears to be an effective general magmatic versus hydrothermal discriminator (Dare et al., 2014; Huang et al., 2019), has similar values for disseminated and vein magnetite in New Afton, where both are present in the same sample (Appendix B). The study of Huang et al. (2019) also showed that hydrothermal magnetite in porphyry systems related to alkaline magmas is characterized by high Mg, Mn, Co, Mo, Sn, and high-field-strength elements. Again, New Afton magnetite exhibits similar content for these elements in disseminated and vein textural types where both are present in the same sample (Appendix B).

Based on geochemical characteristics, the first-order textural distinction of New Afton magnetite into disseminated and vein types does not appear to reflect fundamentally different origins. High values of Ti and V, typical of magmatic magnetite, occur in New Afton vein-type magnetite, which is inferred to be hydrothermal in origin. Conversely, most disseminated grains exhibit many hydrothermal trace-element characteristics, and generally have compositions similar to (or the same as) the compositions of magnetite in veins. These observations suggest similar sources for the two textures, but do not suggest a clear magmatic or hydrothermal origin.

## CONCLUSIONS

A reconnaissance study of magnetite trace-element compositions from the New Afton porphyry Cu-Au deposit was conducted by LA-ICP-MS on a variety of mineralized and unmineralized samples with diverse alteration characteristics. Two textures of magnetite were recognized and analyzed: disseminated, and massive or brecciated veins. Some analyses show anomalously high values of Mg, Al, Si, Ca, and/or P, which are attributed to inclusions of amphibole, quartz, feldspar, or apatite in the sampled magnetite.

Discrimination plots purported to distinguish magmatic and hydrothermal magnetite in porphyry deposits based on statistical treatment of multi-element analyses (Dare et al., 2014; Nadoll et al., 2015; Canil et al., 2016; Huang et al., 2019) were examined; however, the results were contradictory and inconclusive. Multi-element plots indicated traits related to both magmatic and hydrothermal origins. Where both disseminated and vein magnetite are present in samples, the two textures show similar multi-element patterns, suggesting a common origin.

Veins of magnetite define brittle fracture networks, indicating that they crystallized late in the petrogenetic history. The trace-element characteristics of both disseminated and vein magnetite generally conform to those of hydrothermal magnetite in porphyry deposits, but have systematically higher V content, more akin to magmatic magnetite in andesite. These characteristics may reflect relatively high-temperature, oxidized crystallization conditions (Canil et al., 2016). Together, the texture and composition suggest that magnetite crystallized from late magmatic fluids during porphyry mineralization.

## ACKNOWLEDGMENTS

We thank New Gold Inc. for access to drill core and background information. We greatly appreciate critical reviews by N. Rogers and S. Makvandi, which improved the paper.

## REFERENCES

Ballard, J.R., Palin, M.J., and Campbell, I.H., 2002. Relative oxidation states of magmas inferred from Ce(IV)/Ce(III) in zircon: application to porphyry copper deposits of northern Chile; Contributions to Mineralogy and Petrology, v. 144, p. 347–364. https://doi.org/10.1007/s00410-002-0402-5

Bergen, D., Krutzelmann, H., and Rennie, D.W., 2015. Technical report on the New Afton mine, British Columbia, Canada; Roscoe Postle Associates Inc. for New Gold Inc., NI 43-101 report, Project #2400, 256 p.

Canil, D., Grondahl, C., Lacourse, T., and Pisiak, L.K., 2016. Trace elements in magnetite from porphyry Cu-Mo-Au deposits in British Columbia, Canada; Ore Geology Reviews, v. 72, p. 1116–1128. https://doi.org/10.1016/j.oregeorev.2015.10.007

Cooke, D.R., Hollings, P., Wilkinson, J.J., and Tosdal, R.M., 2014. Geochemistry of porphyry deposits. Chapter 14 *in* Volume 13: Geochemistry of mineral deposits; Treatise on geochemistry, 2nd edition, (ed.) S.D. Scott; Elsevier, Oxford, U.K., p. 357–381. https://doi.org/10.1016/B978-0-08-095975-7.01116-5

Dare, S.A.S., Barnes, S.-J., Beaudoin, G., Méric, J., Boutroy, E., and Potvin-Doucet, C., 2014. Trace elements in magnetite as petrogenetic indicators; Mineralium Deposita, v. 49, p. 785–796. https://doi.org/10.1007/s00126-014-0529-0

Griffin, W.L., Powell, W.J., Pearson, N.J., and O'Reilly, S.Y., 2008. GLITTER: data reduction software for laser ablation ICP–MS; *in* Laser ablation-ICP-mass spectrometry in the earth sciences: current practices and outstanding issues, (ed.) P. Sylvester, Mineralogical Association of Canada , Short Course Series, v. 40, p. 308–311.

Huang, X.-W., Sappin, A.-A., Boutroy, E., Beaudoin, G., and Makvandi, S., 2019. Trace element composition of igneous and hydrothermal magnetite from porphyry deposits: relationship to deposit subtypes and magmatic affinity; Economic Geology, v. 114, no. 5, p. 917–952. https://doi.org/10.5382/econgeo.4648

Jochum, K.P., Nohl, U., Herwig, K., Lammel, E., Stoll, B., and Hofmann, A.W., 2005. GeoReM: A new geochemical database for reference materials and isotopic standards; Geostandards and Geoanalytical Research, v. 29, no. 3, p. 333–338. https://doi.org/10.1111/j.1751-908X.2005.tb00904.x

Jochum, K.P., Willbold, M., Raczek, I., Stoll, B., and Herwig, K., 2007. Chemical characterisation of the USGS reference glasses GSA-1G, GSC-1G, GSD-1G, GSE-1G, BCR-2G, BHVO-2G and BIR-1G using EPMA, ID-TIMS, ID-ICP-MS and LA-ICP-MS; Geostandards and Geoanalytical Research, v. 29, p. 285–302. https://doi.org/10.1111/j.1751-908X.2005.tb00901.x

Logan, J.M. and Mihalynuk, M.G., 2014. Tectonic controls on Early Mesozoic paired alkaline porphyry deposit belts (Cu-Au±Ag-Pt-Pd-Mo) within the Canadian Cordillera; Economic Geology, v. 109, no. 4, p. 827–858. https://doi.org/10.2113/econgeo.109.4.827

Logan, J.M., Mihalynuk, M.G., Ullrich, T.D., and Friedman, R., 2006. Geology of the Iron Mask batholith; British Columbia Geological Survey, Open File Map 2006-11, scale 1:25 000.

Mungall, J.E., 2002. Roasting the mantle: slab melting and the genesis of major Au and Au-rich Cu deposits; Geology, v. 30, no. 10, p. 915–918. https://doi.org/10.1130/0091-7613(2002)030%3C0915:RTMSMA%3E2.0.CO;2

Nadoll, P., Angerer, T., Mauk, J.L., French, D., and Walshe, J., 2014. The chemistry of hydrothermal magnetite: a review; Ore Geology Reviews, v. 61, p. 1–32. https://doi.org/10.1016/j.oregeorev.2013.12.013

Nadoll, P., Mauk, J.L., Leveille, R.A., and Koenig, A.E., 2015. Geochemistry of magnetite from porphyry Cu and skarn deposits in the southwestern United States; Mineralium Deposita, v. 50, no. 4, p. 493–515. https://doi.org/10.1007/s00126-014-0539-y

Richards, J.P., 2009. Post-subduction porphyry Cu–Au and epithermal Au deposits: products of remelting of subduction-modified lithosphere; Geology, v. 37, no. 3, p. 247–250. https://doi.org/10.1130/G25451A.1

Richards, J.P., 2011a. Magmatic to hydrothermal metal fluxes in convergent and collided margins; Ore Geology Reviews, v. 40, no 1, p. 1–26. https://doi.org/10.1016/j.oregeorev.2011.05.006

Richards, J.P., 2011b. High Sr/Y arc magmas and porphyry Cu-Mo-Au deposits; Economic Geology, v. 106, no. 7, p. 1075–1081. https://doi.org/10.2113/econgeo.106.7.1075

Rudnick, R.L. and Gao, S., 2003. Composition of the continental crust, Chapter 1 *in* Volume 3: The crust; Treatise on geochemistry, 1st edition, (ed.) R.L. Rudnick; Elsevier-Pergamon, Oxford, U.K., p. 1–64. https://doi.org/10.1016/B0-08-043751-6/03016-4

Sillitoe, R.H., 2002. Some metallogenic features of gold and copper deposits related to alkaline rocks and consequences for exploration; Mineralium Deposita, v. 37, p. 4–13. https://doi.org/10.1007/s00126-001-0227-6

Sillitoe, R.H., 2010. Porphyry-copper systems; Economic Geology, v. 105, no. 1, p. 3–41. https://doi.org/10.2113/gsecongeo.105.1.3

Sinclair, W.D., 2007. Porphyry deposits; *in* Mineral deposits of Canada: a synthesis of major deposit types, district metallogeny, the evolution of geological provinces, and exploration methods, (ed.) W.D. Goodfellow; Geological Association of Canada, Mineral Deposits Division, Special Publication No. 5, p. 223–243.

Tolman, J. and Lipske, J., 2016. Geology and mineralization of the new Afton porphyry Cu-Au deposit and C-zone project update: New Gold presentation to Toronto Geological Discussion Group, <https://s2.q4cdn.com/351510513/files/doc_downloads/New_afton/NewAfton-C-Zone-Presentation_TGDG-Feb16.pdf> [accessed March 26, 2021]

Zhong, S., Seltmann, R., Qu, H., and Song, Y., 2019. Characterization of the zircon Ce anomaly for estimation of oxidation state of magmas: a revised Ce/Ce* method; Contributions to Mineralogy and Petrology, v. 113, p. 755–763. https://doi.org/10.1007/s00710-019-00682-y

# APPENDIX A

## Analyses of trace element concentrations in magnetite in 19 specimens, in various textural settings

This appendix can be found in the file POR-10_Appendix A.xlsx. Values are in parts per million (ppm), as determined by laser-ablation inductively coupled plasma-mass spectrometry. See text for details. This Appendix has not been edited to Geological Survey of Canada specifications.

# APPENDIX B

Multi-element (spider) plots showing New Afton magnetite analyses and the reference field for high-temperature hydrothermal, felsic plutonic, and andesite magnetite compositions, *after* Dare et al. (2014). Sample numbers from Table 1.

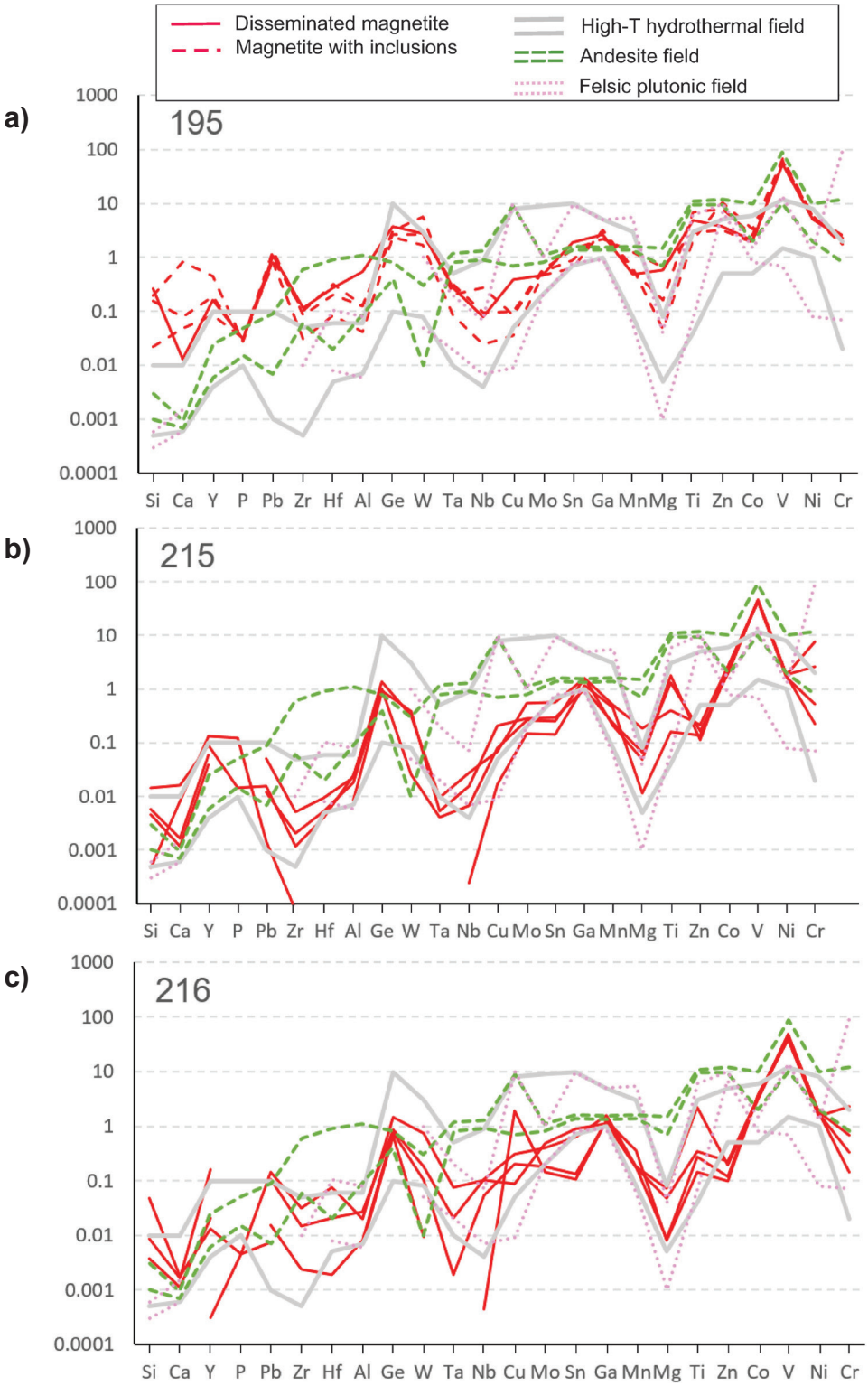


**Figure B1.** Samples with only disseminated magnetite: **a)** sample 195, **b)** sample 215, **c)** sample 216.

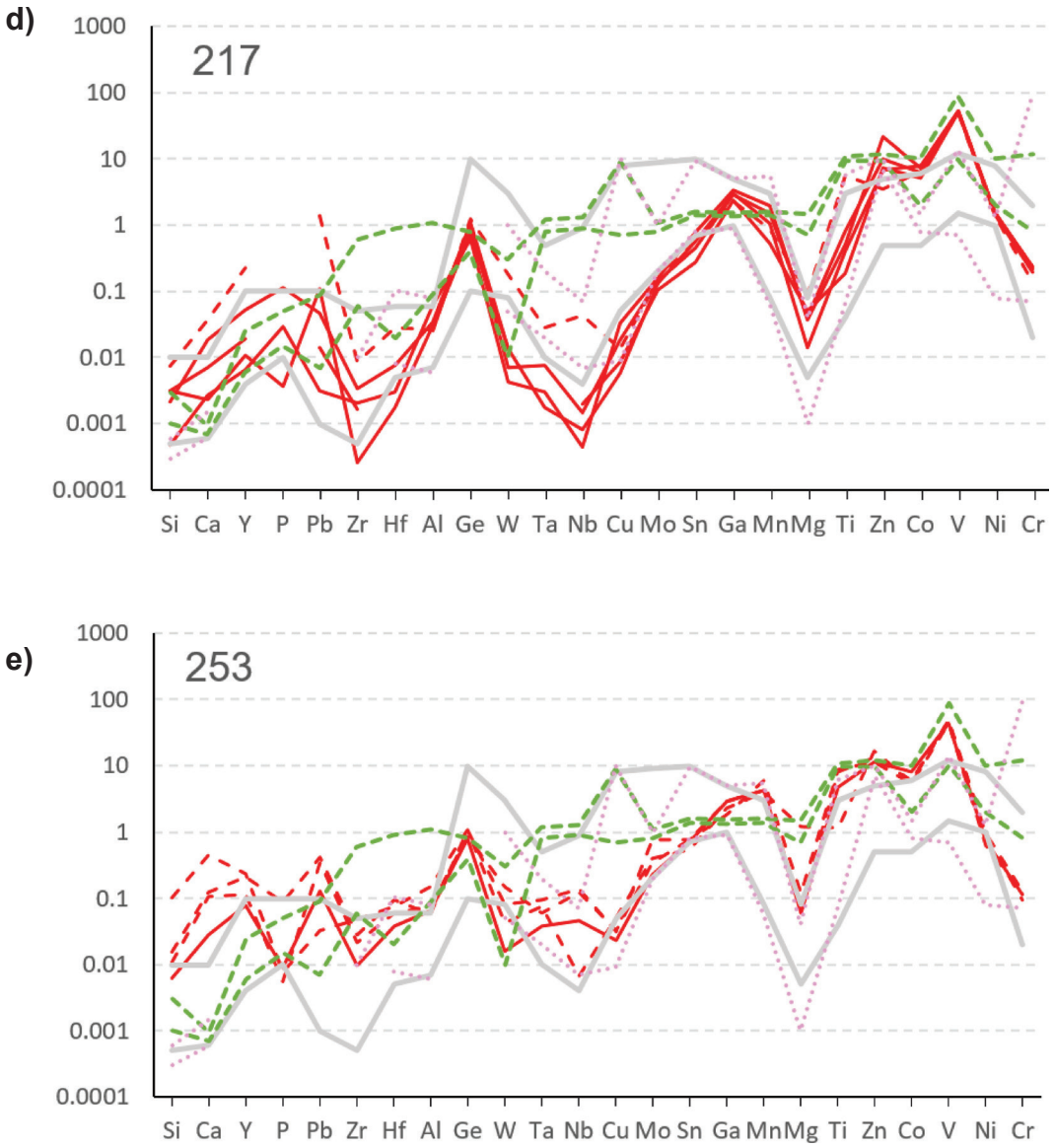


**Figure B1.** (con't) Samples with only disseminated magnetite: **d)** sample 217, **e)** sample 253.

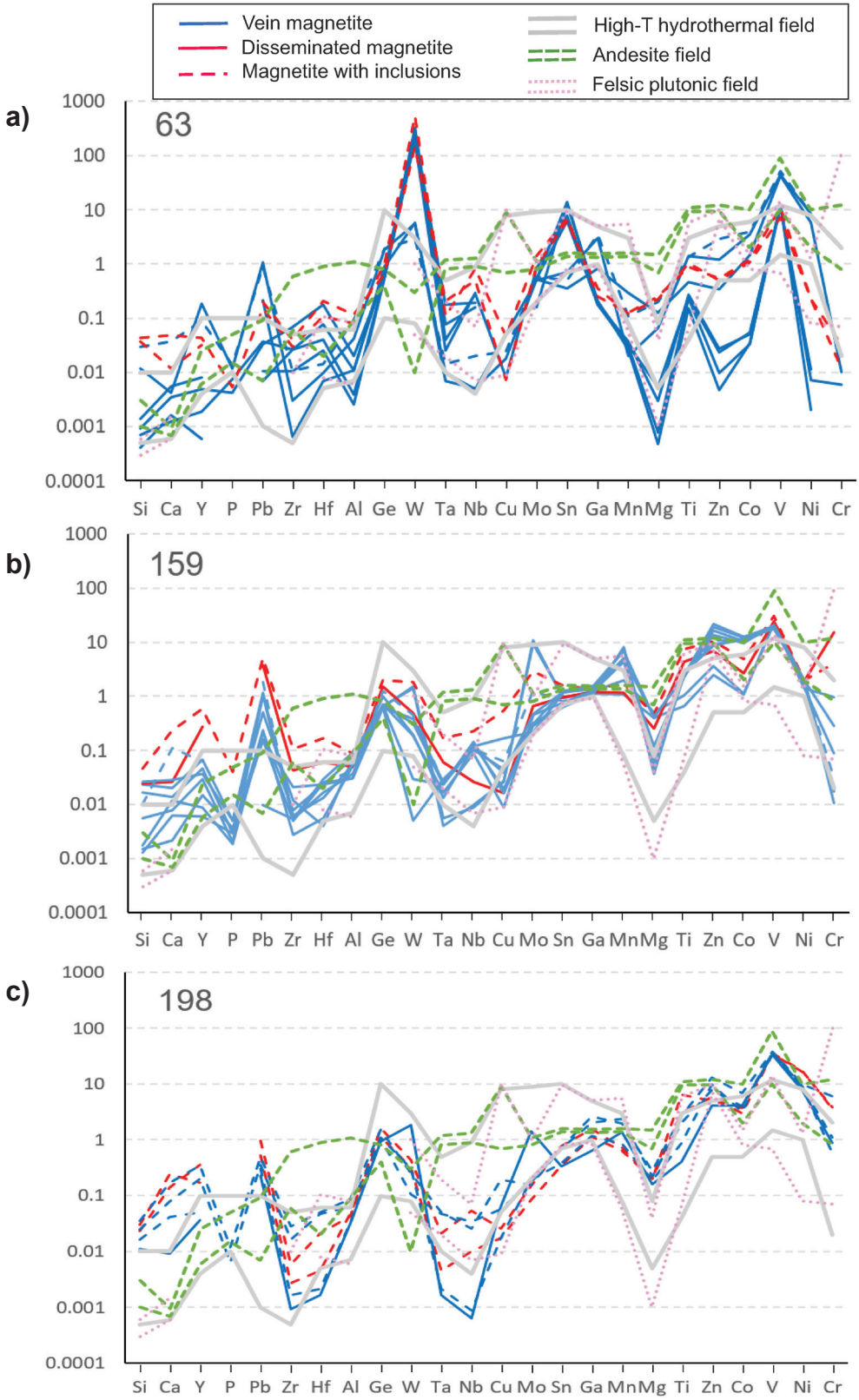


**Figure B2.** Samples with disseminated and vein magnetite: **a)** sample 63, **b)** sample 159, **c)** sample 198.

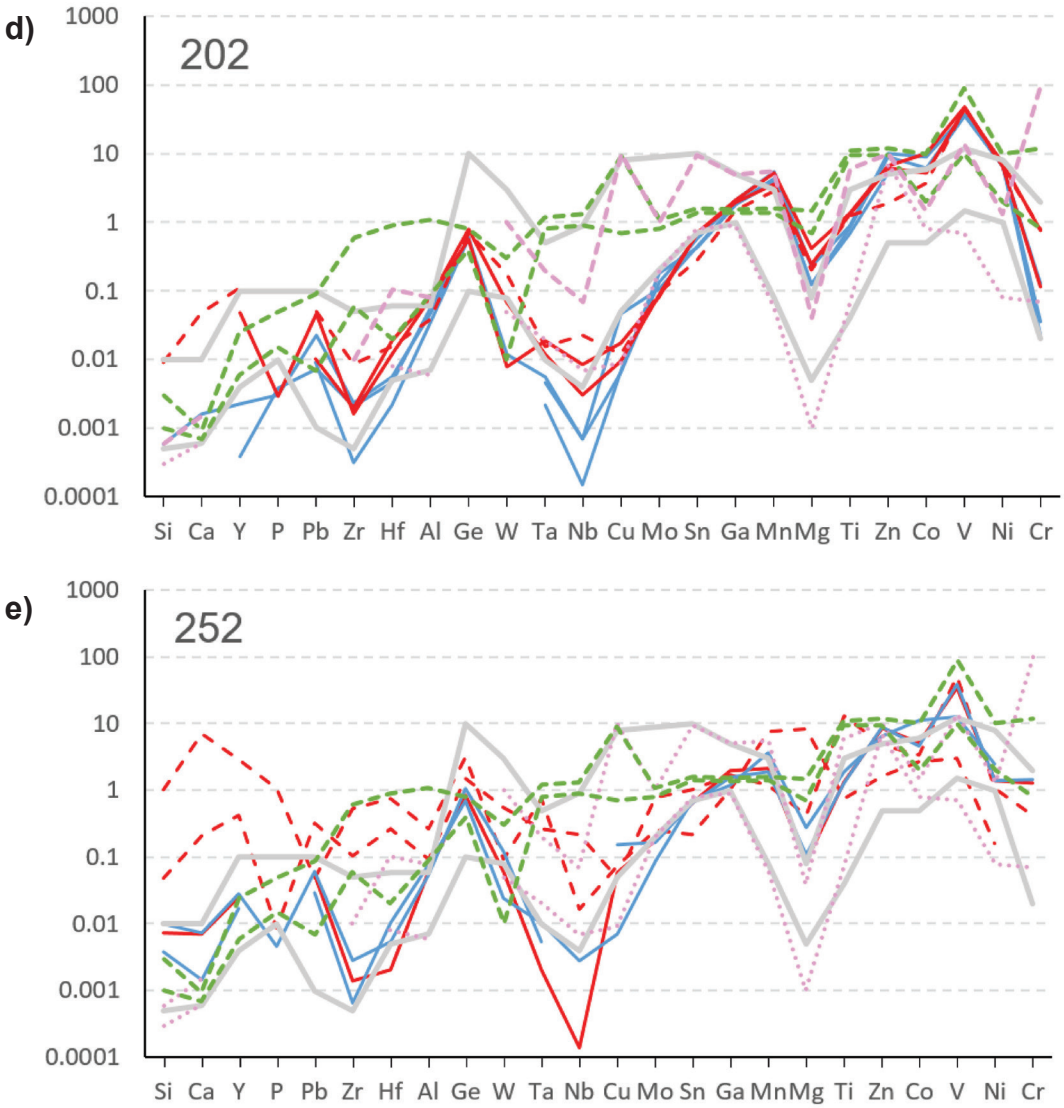


**Figure B2.** (con't) Samples with disseminated and vein magnetite: **d)** sample 202, **e)** sample 252.

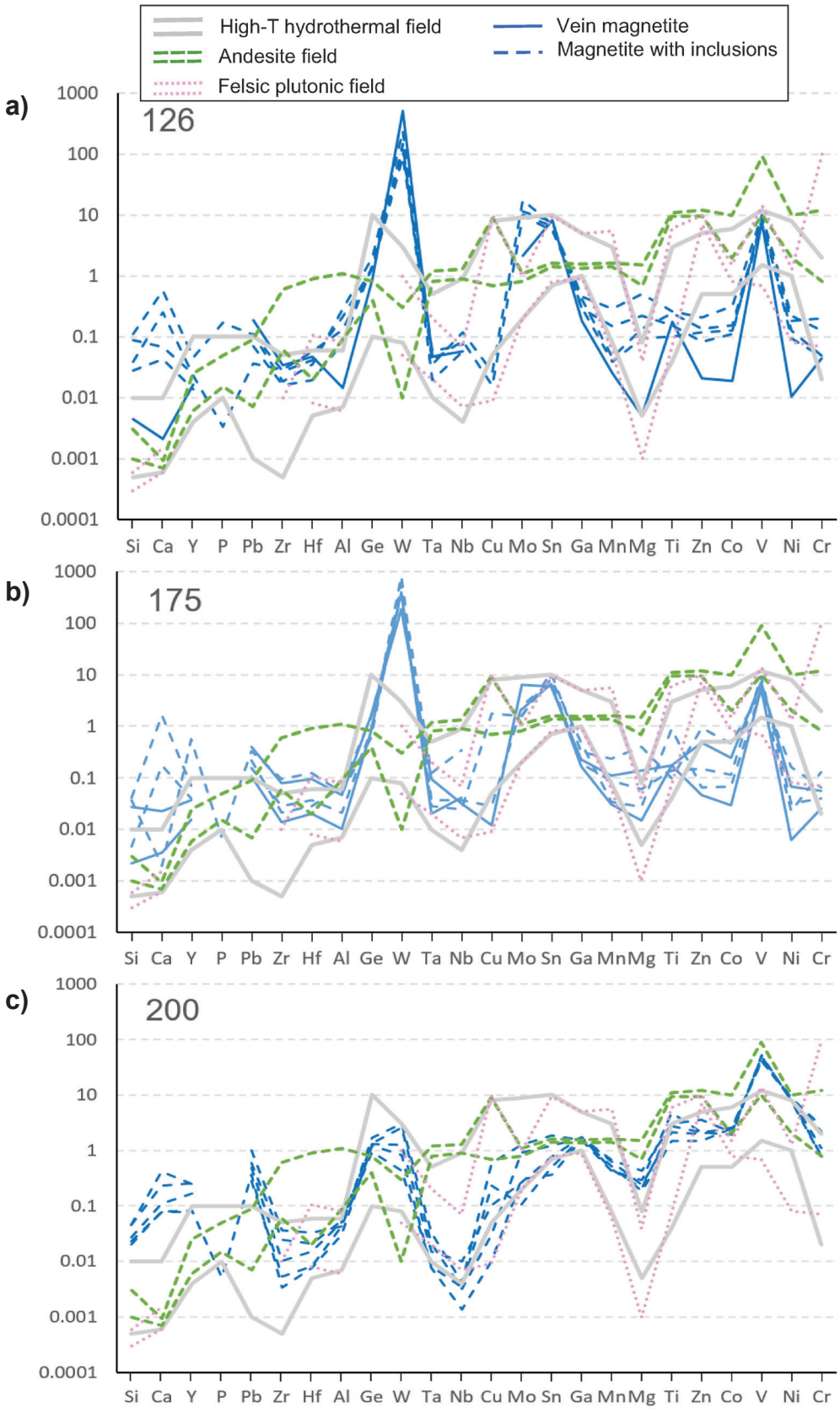


**Figure B3.** Samples with only vein magnetite: **a)** sample 126, **b)** sample 175, **c)** sample 200.

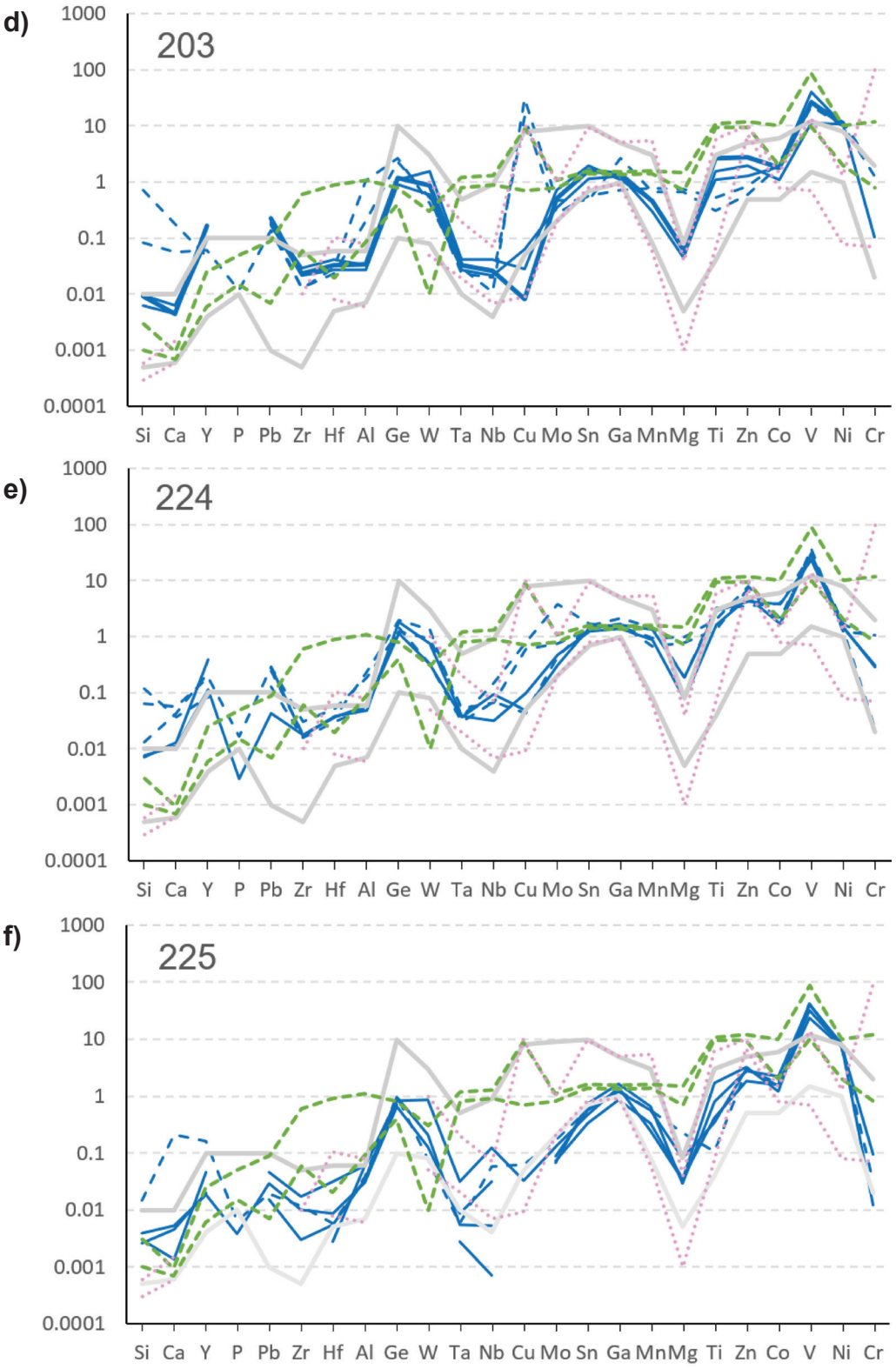


**Figure B3.** (con't) Samples with only vein magnetite: **d)** sample 203, **e)** sample 224, **f)** sample 225.

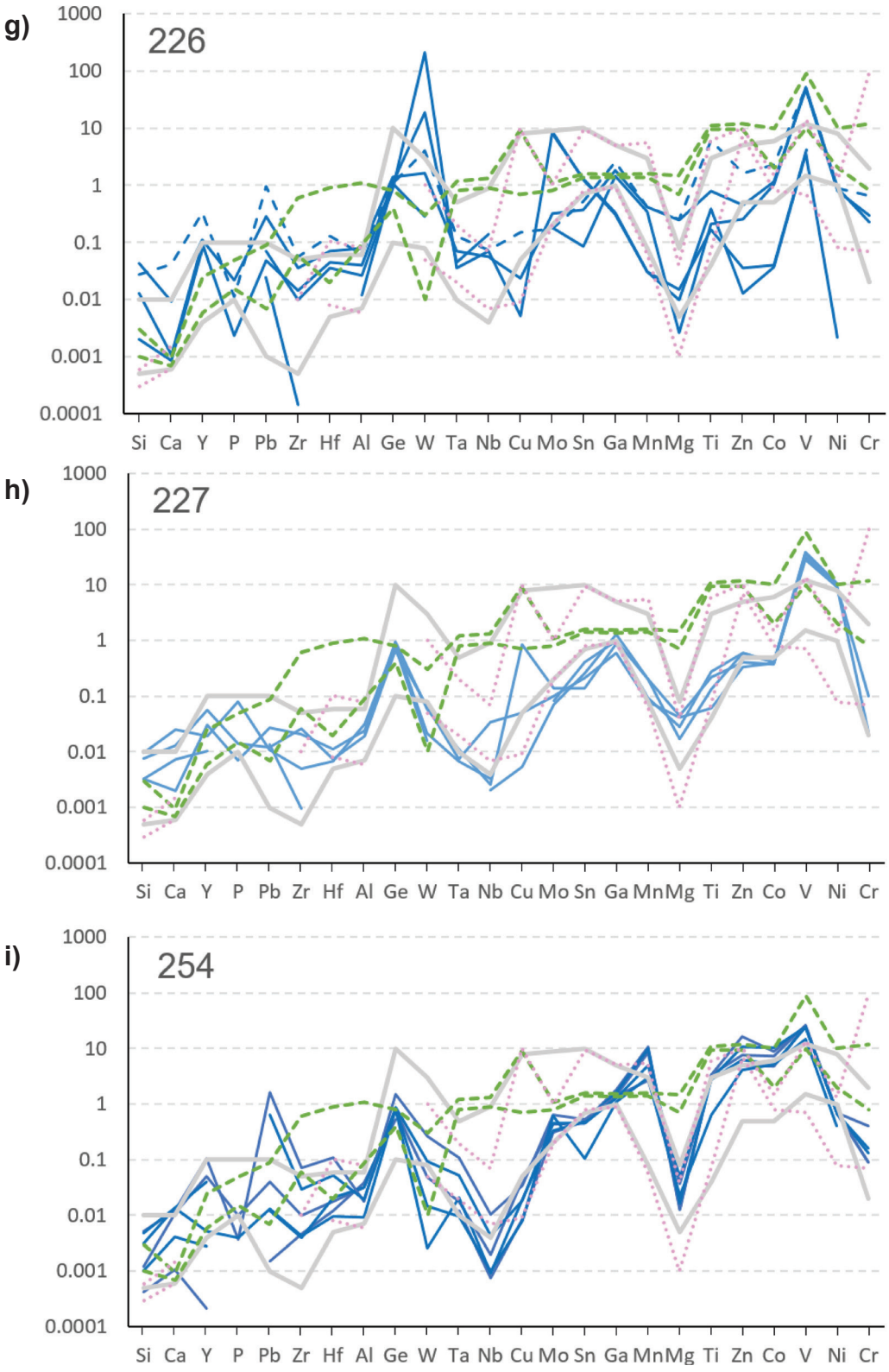


**Figure B3.** (con't) Samples with only vein magnetite: **g)** sample 226, **h)** sample 227, **i)** sample 254.